ESCAPING TRAJECTORIES IN THE HILL THREE BODY PROBLEM AND APPLICATIONS

B.F. Villac
D.J. Scheeres

The University of Michigan
Department of Aerospace Engineering
Ann Arbor, MI 48109-2140
bvillac@umich.edu, scheeres@umich.edu

ABSTRACT *– The structure of low energy escaping trajectories in the Hill three body problem is investigated using a Poincaré map that relates the crossing of a plane containing L_2 back to the first periapsis passage. This set of periapsis is confined in a narrow region which determines the condition of escape from any planetary satellite. In particular, the minimum energy to escape is obtained together with restrictions on the initial conditions (inclination, argument of periapsis and longitude of the ascending node). This leads to a new optimal transfer criterion for the class of directly escaping trajectories. Savings on the order of 190m/s in the case of Europa are obtained when compared to a classic two body model. The results are also extended to the problem of low energy capture. Numerical applications are given for the cases of Miranda, Europa, Titan and Triton.*

KEYWORDS: Hill three body problem, Poincaré map, escape and capture, optimal transfers, libration points.

INTRODUCTION

The present study has been motivated by the Europa Orbiter mission where the end of mission disposal of the spacecraft is an issue for planetary security protection, and escape from Europa at the end of mission has been investigated as a possible solution. This paper is therefore focused on the case of planetary satellite orbiters, even though the results obtained are of wider application since the Hill model used for this analysis also gives a good description of the dynamics of coorbital satellites or, more generally, of two close masses in the gravitational attraction of a larger one ([3]). In this setting, the structure of escaping trajectories having a Jacobi energy just above the critical value of the libration points L_1 and L_2 is investigated, allowing us to draw some practical applications for the design of escape maneuvers. Using the symmetry properties of the Hill model, the results obtained are also directly applicable to the related problem of low energy capture trajectories which can model the accretion properties of a planet in formation. We know from classical results on the circular restricted three body problem (CR3BP) that escape is only possible when the zero velocity surface opens at L_1 or L_2, setting up a minimal value of the Jacobi integral for escape. In this paper, trajectories are considered to have escaped from the primary under consideration when they cross

the opening close to L_1 or L_2 with a positive outward velocity. The analysis is therefore focused on the dynamics close to the primary, which justifies the use of the Hill three body problem (H3BP) as the underlying model. Moreover, the assumptions of this model are met for most planetary satellites of interest in the solar system, which makes this model well suited for the investigation of practical applications (see [6]). A Poincaré map is used to relate the crossing of the escaping trajectories through a plane containing the libration points with the previous periapsis radius vector of those trajectories. This computation is made for constant values of the Jacobi energy, allowing us to reduce the dimensionality of the system. The resulting set of periapsis points that lead to escape is confined to a narrow region, symmetric about the equatorial plane, which can be used to determine the minimum energy required to escape from the satellite. In particular, the minimal ΔV to escape from the surface of a few planetary satellites (Europa, Titan, Miranda and Triton) is given. Constraints on the minimal energy and the initial conditions required for escaping are hence obtained and a new optimal escape criterion can be deduced for the restricted class of directly escaping trajectories starting in a low circular orbit and using a single impulsive maneuver. Hénon showed in [4] that quasi-circular periodic orbits exist in the planar H3BP. These orbits have also been proven to be stable. For non-zero inclination, Scheeres et al. showed in [6] that below a critical inclination ($\simeq 45^o$), low circular orbits are stable about most planetary satellites in the solar sytem. These orbits have periodic variations in eccentricity which can be neglected at first approximation in the case of low altitude trajectories. Therefore, at low altitudes, we can assume that a spacecraft is in a Keplerian circular orbit and investigate how much ΔV is needed for this spacecraft to escape. In this paper, we prove that the minimum ΔV to escape is obtained for tangential burns at a specified point in the orbit and that this minimum decreases as altitude increases. The optimality of these transfers is then proven for the class of directly escaping trajectories using one or two impulsive maneuvers. Given an initial altitude, the optimal Jacobi constant and the minimum ΔV required to reach escape are obtained from a graph. The time of the maneuver is determined by a condition on the longitude of the ascending node and the argument of periapsis of the transfer trajectory (taken at periapsis). Restrictions on the inclination for these transfers to be possible also exist, as the initial orbit must be near-equatorial. Fuel savings on the order of 190 m/s in the case of Europa can be obtained, as compared to a two body Keplerian model. A simple scaling of these results allows us to map our analysis to any planetary satellite (assuming the Hill model). Numerical applications are given for the cases of Miranda, Europa, Titan and Triton, which cover the three typical cases emerging from the analysis.

HILL THREE BODY DYNAMICS

The circular restricted three body problem (CR3BP) describes the dynamics of a massless object attracted by two point masses revolving around each other in a circular orbit. This model has found many applications in both astronomy and astrodynamics, indeed, it is the simplest model of the main perturbation of an object in interplanetary space (e.g. comet, Jupiter, Sun sytem) or even for Earth orbiters for high enough altitude (see [5], p55). In particular, this model gives a good description of the dynamics around a planetary satellite. However, in this case when the dynamics is considered close to the smaller primary, the Hill three body model viewed as a limiting case of the CR3BP also gives a good description of the dynamics and consists of a simpler set of equations (without any free parameters). The Hill model has, however, a much wider generality since it also covers the dynamics of two small masses in a circular orbit about a larger one. In particular, the Hill model gives a good description of the dynamics of coorbital satellites and can be used to describe the dynamics in planetary rings or the accretion properties of planets in formation (see [3]).

Equations of motion

The Hill model can be obtained from the CR3BP by taking the center of the coordinate system to be at the center of the smaller primary and letting the mass ratio of the primaries go to zero while scaling the coordinates to remain finite (see [1] for example). The resulting equations of motion can be written as:

$$\ddot{x} - 2N\dot{y} = -\frac{\mu}{r^3}x + 3N^2x \tag{1}$$

$$\ddot{y} + 2N\dot{x} = -\frac{\mu}{r^3}y \tag{2}$$

$$\ddot{z} = -\frac{\mu}{r^3}z - N^2z \tag{3}$$

where N is the angular velocity of the motion of the primaries around each other, μ is the gravitational parameter of the attracting body of interest and $r = \sqrt{x^2 + y^2 + z^2}$ (see Figure 1). Note that for $N = 0$, the previous equations reduce to the classical two body problem.

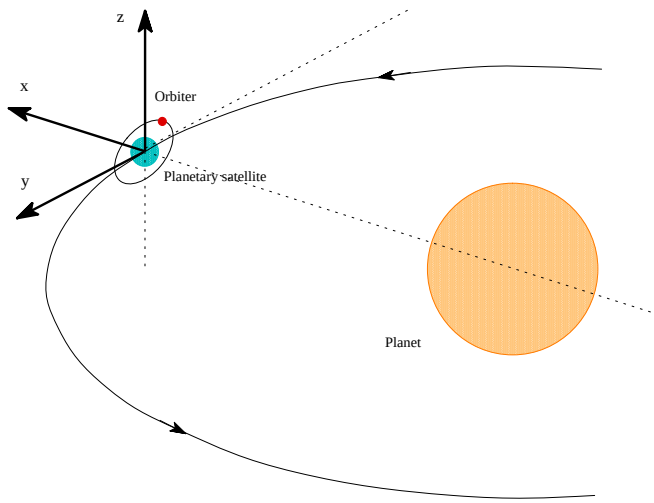

Figure 1: Geometry of the Hill problem in the case of Europa

We immediately see that the solutions $x = \pm\left(\frac{\mu}{3N^2}\right)^{1/3}$, $y = z = \dot{x} = \dot{y} = \dot{z} = 0$ are particular solutions of these equations. They correspond to the analog of the Lagrangian points L_1 and L_2 in the CR3BP, but are now symmetric about the origin (L_1 is the point with negative abscissa and L_2 is the one with positive abscissa _ see Figure 2).

Zero velocity surfaces and escape

Similar to the CR3BP, the Hill model has a nontrivial integral of motion, the Jacobi constant J.

$$J = \frac{1}{2}v^2 - \frac{\mu}{r} - \frac{1}{2}N^2(3x^2 - z^2) \tag{4}$$

where $v = \sqrt{\dot{x}^2 + \dot{y}^2 + \dot{z}^2}$ is the speed of the particle. This constant has deep consequences for the dynamics of the motion. In particular, the physical condition $v \geq 0$ in (4) imposes a restriction on the allowable position space for the motion at any given value of J. Setting $v = 0$, (4) gives the implicit definition of a surface upon which the velocity is zero, thus delimiting the physical boundary of allowable motion (see Figure 2).

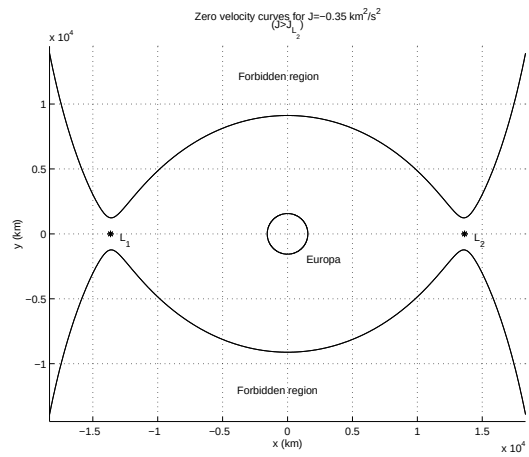

Figure 2: Zero velocity surfaces in the case of Europa (planar case)

In our case it also gives a minimum threshold that must be reached for escape to occur. More precisely, escape becomes possible for $J > J_{L_{1,2}}$ where

$$J_{L_{1,2}} \quad = \quad -\frac{1}{2}\left(9\mu N\right)^{2/3} \tag{5}$$

This corresponds to the critical value of J for which the zero velocity surfaces open at L_1 and L_2. Escaping trajectories are those that cross either plane $x = x_{L_{1,2}}$ in the outward direction. We will analyse some characteristics of these trajectories with a Jacobi constant just above the critical value of $J_{L_{1,2}}$, corresponding to the lowest energy escaping trajectories possible.

Symmetries and extension to the capture problem

As a limiting case of the CR3BP, the Hill model takes advantage of the "almost symmetries" present in the CR3BP and turns them into exact mathematical symmetries. In particular, the equilibrium points L_1 and L_2 become symmetric about the origin.

More precisely, if $(x, y, z, \dot{x}, \dot{y}, \dot{z}, t)$ denotes a solution of the equations of motion, then the trajectories obtained by applying the following transformations are also valid solutions:

$$(x, y, z, \dot{x}, \dot{y}, \dot{z}, t) \quad \xrightarrow{S_1} \quad (-x, y, z, \dot{x}, -\dot{y}, -\dot{z}, -t) \tag{6}$$

$$(x, y, z, \dot{x}, \dot{y}, \dot{z}, t) \quad \xrightarrow{S_2} \quad (x, -y, z, -\dot{x}, \dot{y}, -\dot{z}, -t) \tag{7}$$

$$(x, y, z, \dot{x}, \dot{y}, \dot{z}, t) \quad \xrightarrow{S_3} \quad (x, y, -z, \dot{x}, \dot{y}, -\dot{z}, t) \tag{8}$$

The composition of these three symmetries yield other symmetries, notably the composition of (1),(2) and (1),(2),(3) yield:

$$(x, y, z, \dot{x}, \dot{y}, \dot{z}, t) \quad \xrightarrow{S_4} \quad (-x, -y, z, -\dot{x}, -\dot{y}, \dot{z}, t) \tag{9}$$

$$(x, y, z, \dot{x}, \dot{y}, \dot{z}, t) \quad \xrightarrow{S_5} \quad (-x, -y, -z, -\dot{x}, -\dot{y}, -\dot{z}, t) \tag{10}$$

This last symmetry is a pure symmetry about the origin which results in the symmetry of L_1 and L_2. Also from S_5 we see that if $\mathcal{X} = (x, y, z, \dot{x}, \dot{y}, \dot{z}, t)$ is an escaping trajectory about L_2, then $S_5(\mathcal{X})$ is an escaping trajectory about L_1. In other words, if $P(\mathcal{X})$ is a property of an L_2-escaping trajectory, then $S_5(P(\mathcal{X}))$ will be the corresponding property of the L_1-escaping trajectory. Therefore, we have a 1-1 correspondance between L_1 and L_2 and we can restrict the analysis to L_2-escaping trajectories.

From S_3, we see that the same is true for reflections about the (x, y)-plane, allowing us to restrict the analysis to escaping trajectories having a positive z-coordinate. This result will be used to simplify the computation of the Poincaré map.

The symmetries S_1 and S_2 involve a reflection in time, indicating that if $\mathcal{X}$ is an escaping trajectory, then $S_{1,2}(\mathcal{X})$ will be a capture trajectory. By this, we mean trajectories coming from the exterior region and crossing the planes $x = x_{L_{1,2}}$ with an inward velocity. These trajectories have at least one of their periapsis in the Hill region, but are not necessarily captured for long periods of time. As some examples will show, these trajectories may directly impact the planetary satellite under consideration. Thus, applying S_1 or S_2 to escaping trajectories, we immediately obtain a corresponding characterisation for capture trajectories.

Normalisation and scaling to any planetary satellite

Besides these symmetry properties, the form of the Hill equations of motion allows for the nondimensionalization of the model and elimination of all free parameters. More precisely, by taking $l = \left(\frac{\mu}{N^2}\right)^{1/3}$ as the unit length and $\tau = \frac{1}{N}$ as the unit time, the equations of motion transform into the following parameterless equations:

$$\ddot{x} - 2\dot{y} = -\frac{x}{r^3} + 3x \tag{11}$$

$$\ddot{y} + 2\dot{x} = -\frac{y}{r^3} \tag{12}$$

$$\ddot{z} = -\frac{z}{r^3} - z \tag{13}$$

Note that from a formal point of view, all dimensional quantities are nondimensionalized by taking $N = 1$ and $\mu = 1$. For example, in the nondimensional setting, we have:

$$J_{L_{1,2}} = -\frac{1}{2}(9)^{2/3} = -2.163... \tag{14}$$

$$x_{L_{1,2}} = \pm\left(\frac{1}{3}\right)^{1/3} = \pm 0.693... \tag{15}$$

All computations performed on Equations (11),(12) and (13) can be directly scaled to any physical system modeled by the Hill equations by simply scaling of the results. In particular, all the analysis which follows applies to most planetary satellite of interest in the solar system as was previously indicated in [6]. Table 1 gives the length and time scale for Miranda, Europa, Titan and Triton.

Table 1: Physical parameters for Miranda, Europa, Titan and Triton (computed from [2])

Satellite (planet)	μ (km^3/s^2)	Orbital period $(days)$	Length scale (km)	Time scale (hr)	Radius (km)	Normalized radius
Europa (Jupiter)	3202.8 ±13.3	3.551	19692	13.56	1569 ± 10	0.079
Titan (Saturn)	8979.3 ± 2.0	15.945	75576	60.90	2575 ± 2	0.034
Miranda (Uranus)	4.73	1.413	1214	5.39	242 ± 5	0.199
Triton (Neptune)	8674.3 ±1668	5.877 (Retrograde)	38406	22.44	1750 ± 250	0.045

In the remainder of this paper computations will be performed in the nondimensional setting, and some applications will be given for the four cases indicated above.

Note that the scaling depends both on the physical parameters of the primaries as well as their orbital characteristics (mean motion N). Therefore, planetary satellites of different mass and radius may have the same radius in nondimensionalized coordinates. Figure 3 shows the different normalized radii for the four satellites considered.

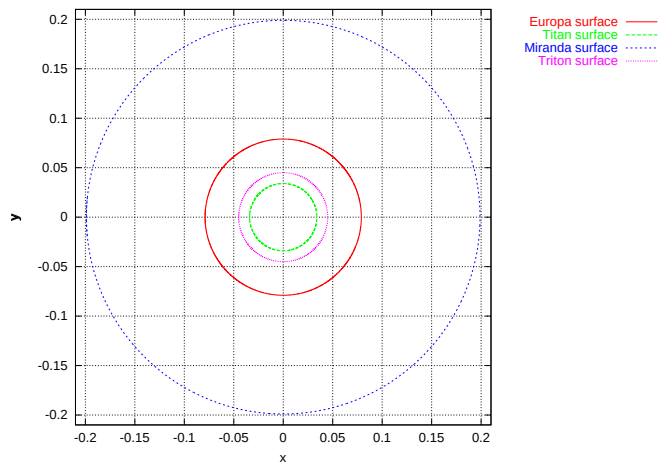

Figure 3: Surfaces of Europa, Titan, Miranda and Triton in nondimensional scale

POINCARÉ MAP

A Poincaré map generally refers to the association of a discrete time system given an initial, more complicated, continuous time dynamical system. It allows us to reduce the dimensionality of the system by at least one, and two if there exists a first integral, as is the case in the Hill model. Our use of a Poincaré map will be mostly numerical, giving us a convenient way to represent some properties of the flow and allowing us to numerically extract some constraints on initial conditions.

While generally applied to periodic orbits or to study the structure of flows near homoclinic/heteroclinic trajectories (see [7] for example), the definition of a Poincaré map really requires only the choice of two surfaces of sections transversal to the flow in phase space, and can be used in more general ways. This study of the Poincaré map is the study of a discrete map from one surface of section to the next one (see Figure 4).

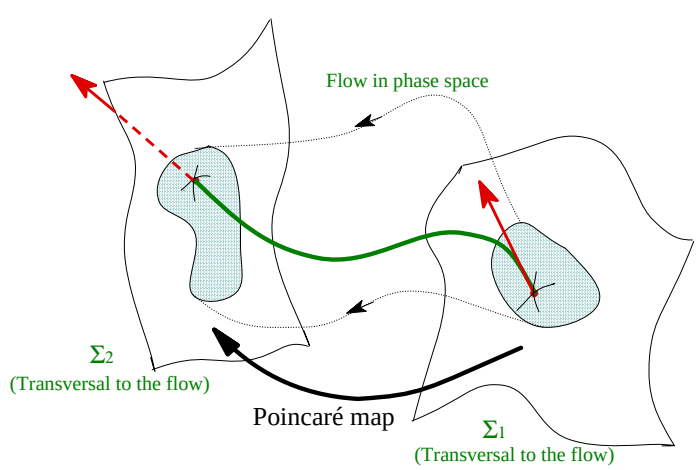

Figure 4: Concept of a Poincaré map

Computation of the map

For our purpose, we use a map relating escaping trajectories (i.e., having $\dot{x} > 0$ at $x = x_{L_2}$ near the equilibrium L_2) back to their first periapsis. The initial surface of section Σ_1 is hence the cross-section of the plane $x = x_{L_2}$ with the Hill region and the image surface Σ_2 being the set defined by the periapsis condition $\dot{r} = 0$ and $\ddot{r} > 0$ prior to Σ_1. The transversality of these surfaces of section with the flow generated by the equations of motion is proven in [8]. As mentioned earlier, there exists an integral of motion in the model which allows us to reduce the dimensionality of the map by an additional dimension. The Poincaré map is computed at a given value of the Jacobi integral J, which makes this map a function of J.

In the 3 dimensional case, the resulting Poincaré map is 4 dimensional, which means that we need four parameters to parametrize Σ_1 and Σ_2. On Σ_1 we consider the (y, z) coordinates in the plane $x = x_{L_2}$ plus two angles for the direction of the velocity vector, whose magnitude is determined by the Jacobi constant. With this parameterization, the inital conditions on Σ_1 can be written as:

$$x_0 = x_{L_2} \quad ; \quad \dot{x_0} = v \cos\phi \cos\delta \tag{16}$$

$$y_0 = y \quad ; \quad \dot{y_0} = v \cos\phi \sin\delta \tag{17}$$

$$z_0 = z \quad ; \quad \dot{z_0} = v \sin\phi \tag{18}$$

where $v = \sqrt{2(J + 1/r) + (3x^2 - z^2)}$ (nondimensionalized case), $-\pi/2 < \delta < \pi/2$ and $-\pi/2 < \phi < \pi/2$.

On Σ_2 we use three spatial coordinates (either (x, y, z) or (r_p, ω, Ω), the periapsis radius, argument of periapsis and longitude of the ascending node) plus the inclination. This is merely a convenient way to obtain practical numerical conditions on escape. From a graphical point of view, Figure 8 give the projection of the image of the Poincaré map onto position space.

Note that in the planar case, the Poincaré map requires only 2 parameters on Σ_1 and Σ_2. We choose y and δ on Σ_1 and (x, y) (or equivalently $(r_p, \tilde{\omega})$, periapsis radius and longitude of periapsis) on Σ_2. Figure 5 shows the geometry of the Poincaré maps considered in the planar case.

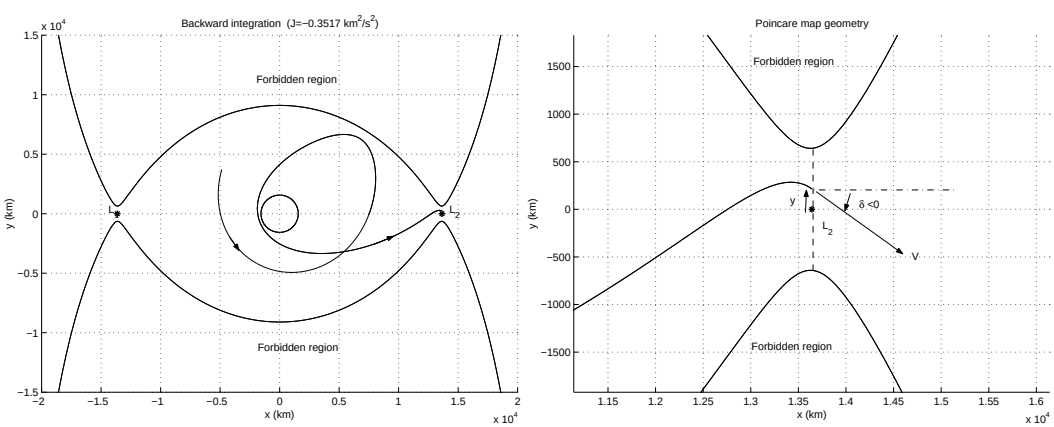

Figure 5: Computation of the Poincaré maps in the planar case

Given the initial conditions (16), (17) and (18), a $7 - 8^{th}$ order Runge-Kutta-Fehlberg integration routine is used to integrate the trajectories backward to Σ_2. The initial points are chosen randomly on Σ_1. Symmetry S_3 is used to restrict the computation to the points $z > 0$, the symmetric points being obtained by directly applying the symmetry at periapsis. Examples of Poincaré maps at several Jacobi constant value are given in Figure 10.

Results

The Poincaré maps have been computed with 100×100 points in the planar case and 300×300 points in the 3 dimensional case. The values of J vary from $J_{L_2} + 10^{-9}$ to $J_{L_2} + 0.11$.

Figure 6 gives an example of a Poincaré map for $J = -2.16$ in the planar case, together with two close-ups. As appears immediately on these figures, the image of the Poincaré map is divided into two (numerically) disjoint sets of points denoted Σ_2^a and Σ_2^b. The first one, Σ_2^a, oval shaped, is close to the primary and confined to a small region of altitude and longitude of periapsis, and corresponds to trajectories that come from the neighborhood of the primary. The second set of points, Σ_2^b, is confined close to L_2 and corresponds to trajectories coming from the exterior region before exiting again (see Hénon and Petit [3]).

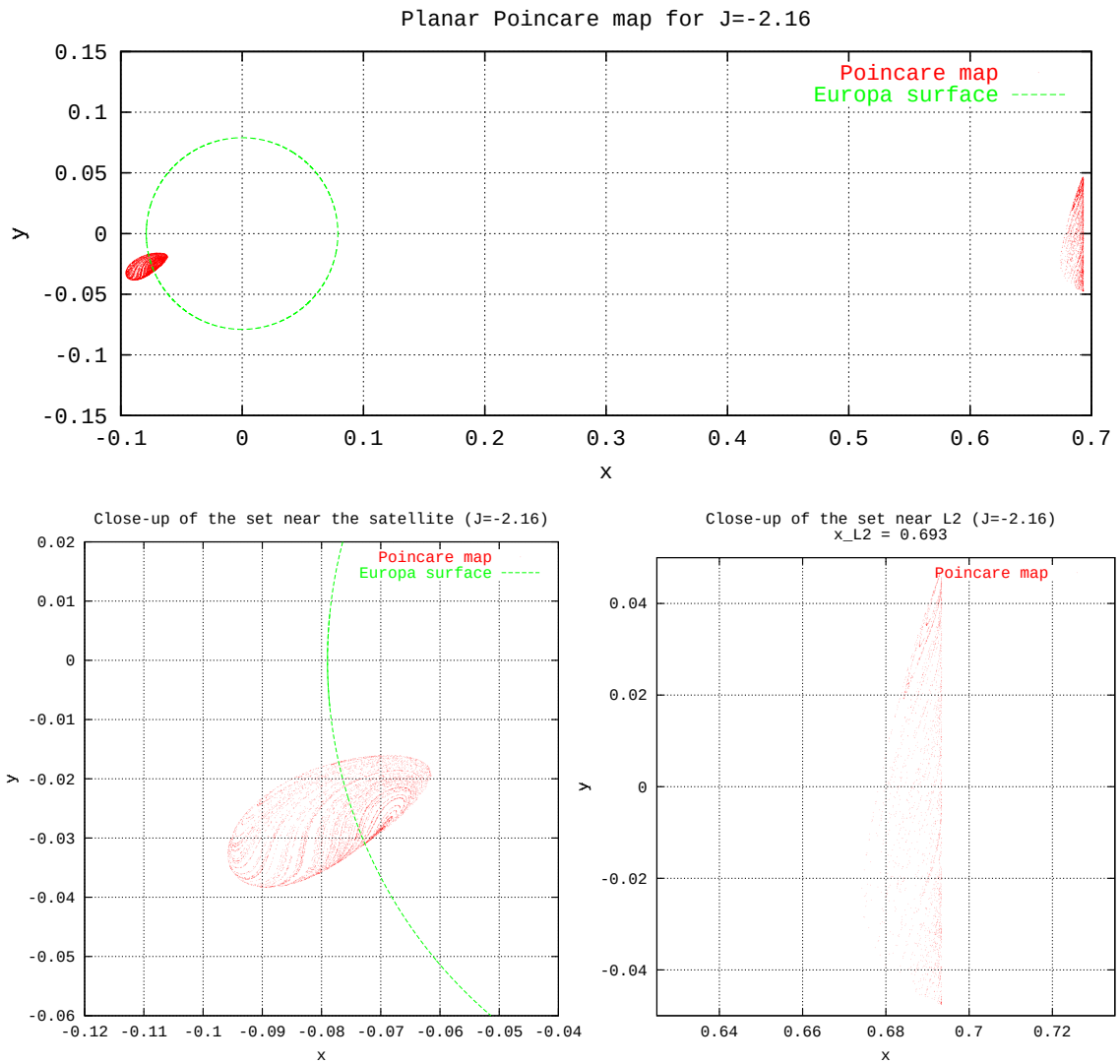

Figure 6: Example of a planar Poincaré map for $J = -2.16$

Figure 7 illustrates the different types of trajectories encountered in the case of Europa. From a practical point of view, we will consider only the first region, Σ_2^a, in the remainder of our investigation, since it is the most important for the pratical application of escape conditions for a planetary satellite orbiter.

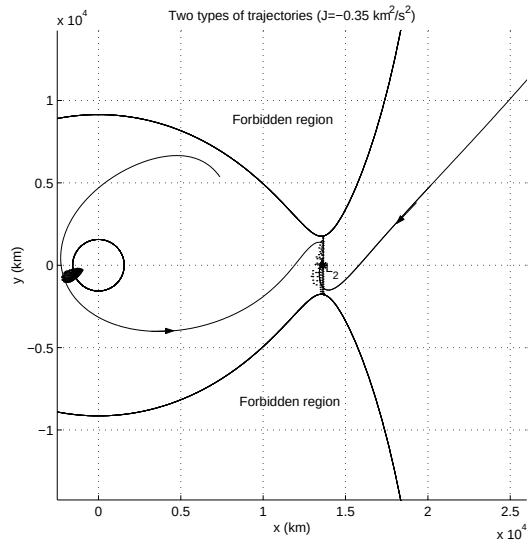

Figure 7: Types of trajectories encountered

Figures 8 and 9 give a representation of the Poincaré map obtained with the same value of J but now in 3 dimensional space. Notably, the (x, z) projection clearly shows the symmetry about the equatorial plane (as expected from S_3) and the (r, i) projection indicates the range of inclinations covered by the velocity vectors. We can see from these results that the extrema of radius and longitude of the ascending node in Σ_2^a are reached in the equatorial plane and the maximum of inclination is reached for $r < r_{L_2}$, the periapsis of the stable manifold associated with L_2.

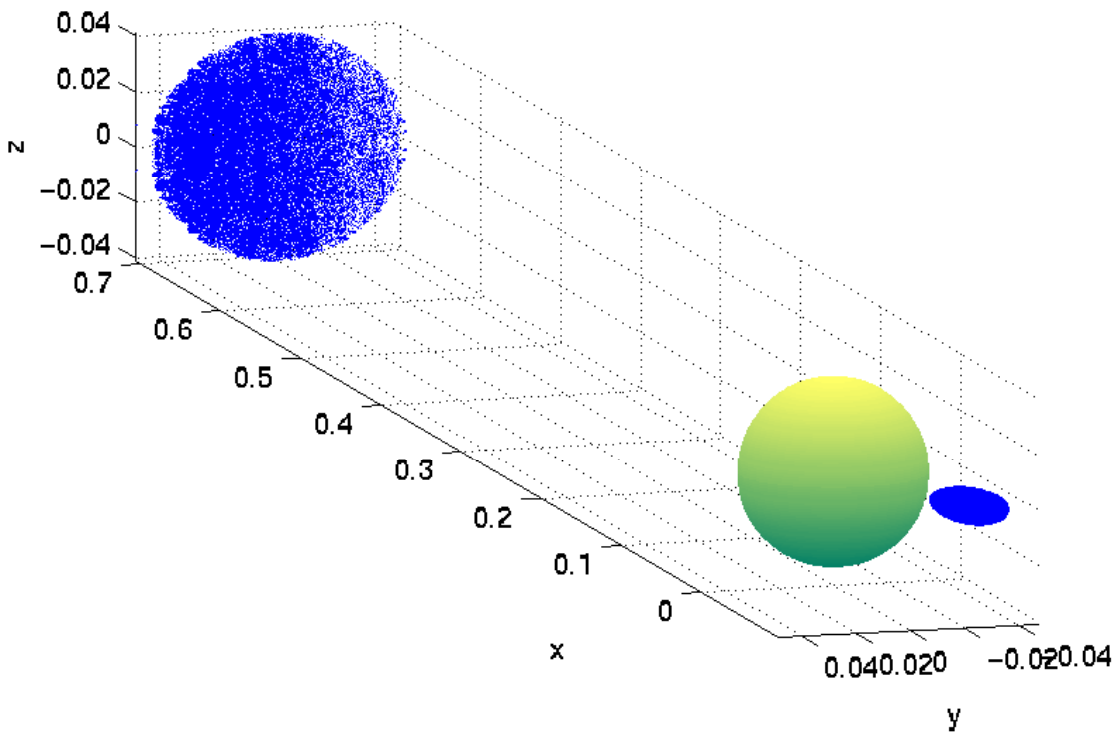

Figure 8: Example of a Poincaré map in 3 dimensions with Titan (J=-2.16)

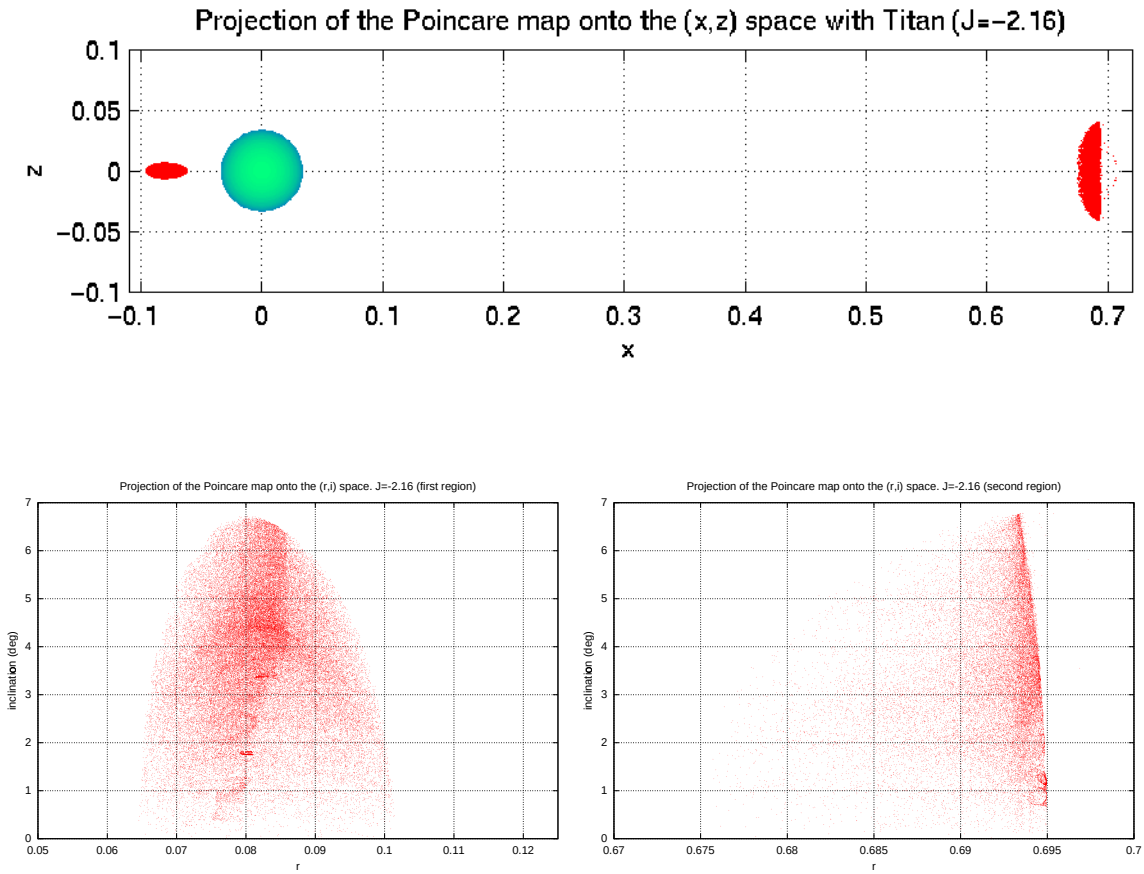

Figure 9: Projection fo a Poincaré map on the (x, z) and (r, i) spaces case

Figure 10 shows a series of Poincaré maps at different values of Jacobi constant. It immediately appears on these figures that the set of points defining the Poincaré map enlarges as the Jacobi constant increases from J_{L_2}. At the limit, when $J \simeq J_{L_2}$, the Poincaré map reduces to a point which corresponds to the periapsis of the stable manifold associated with L_2. Formally, this allows us to classify all the planetary satellites according to whether or not this periapsis is above or below their physical surface. Miranda is of type 1 (periapsis below the surface), Titan and Triton are of type 2 (periapsis above the surface) and Europa is the exceptional case; the periapsis of the unstable manifold lies at the surface of Europa. We see that for type 1 satellites, it is possible to directly escape the surface of the body at the minimal energy necessary to escape, J_{L_2}, by performing an impulsive thrust at the surface, while for type 2 satellites, one need to go to higher energies to directly escape (see also section "Optimal Transfers"). This classification has also some consequences for the capture problem, as is discussed later.

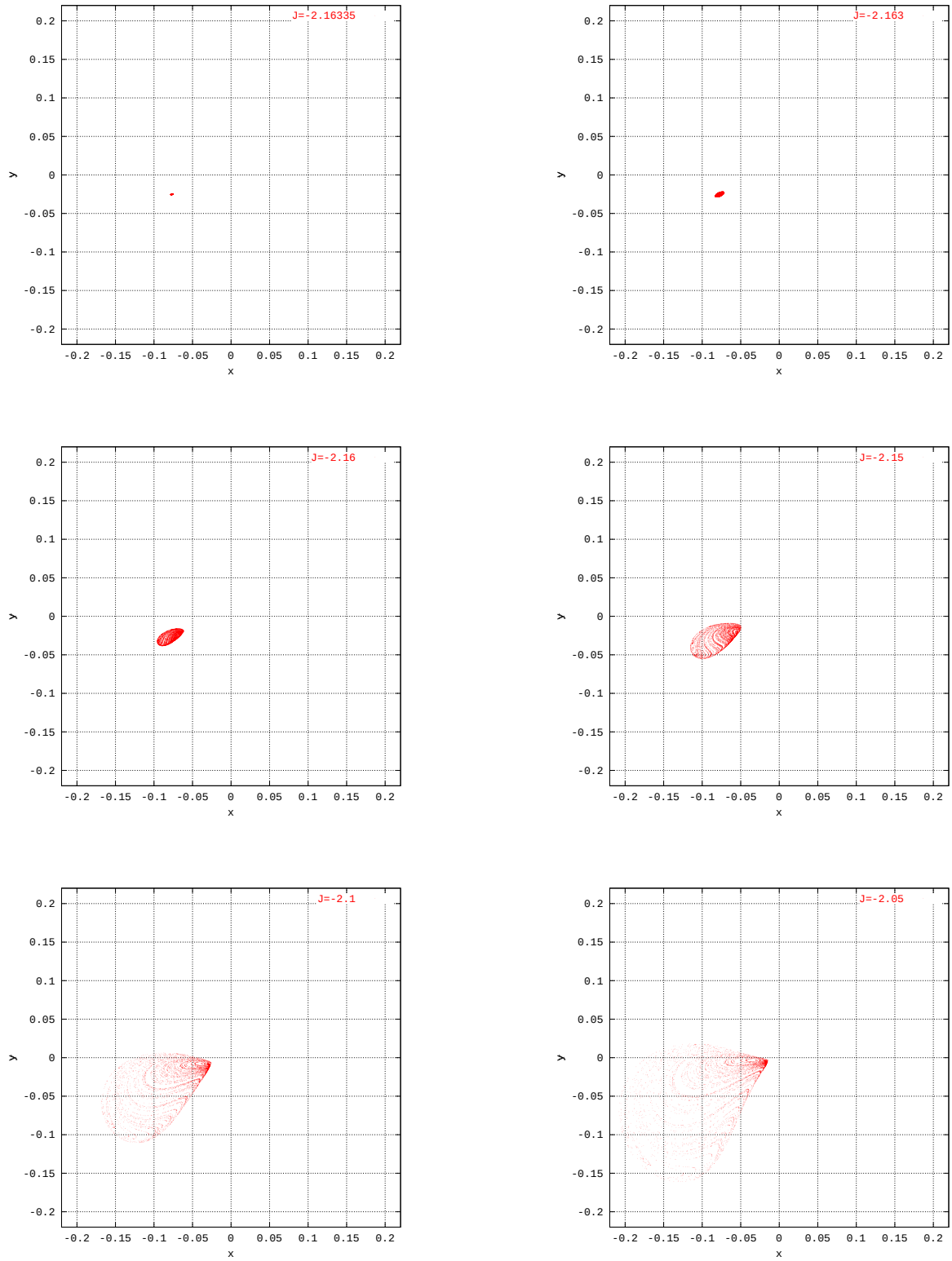

Figure 10: Series of Poincaré maps (Σ_2^a) at several values of the Jacobi constant

As noted above, as J varies the characteristics of the Poincaré maps vary. Some of these variations are captured in Figures 11 and 12 which show the extrema of the radius, longitude of periapsis (long. of the ascending node in 3D), eccentricity and inclination as a function of J. Note that all these extrema are reached in the equatorial plane. In particular, this corresponds to the condition $\omega = 0^o$ in the 3 dimensional case.

These graphs show that the set of first periapsis before escape, Σ_2^a, is confined in a rather narrow region even for large values of J. At $J = -2.05$, the opening at L_2 is 4 to 5 times the radius of Europa while Σ_2^a extends over less than 3 radius.

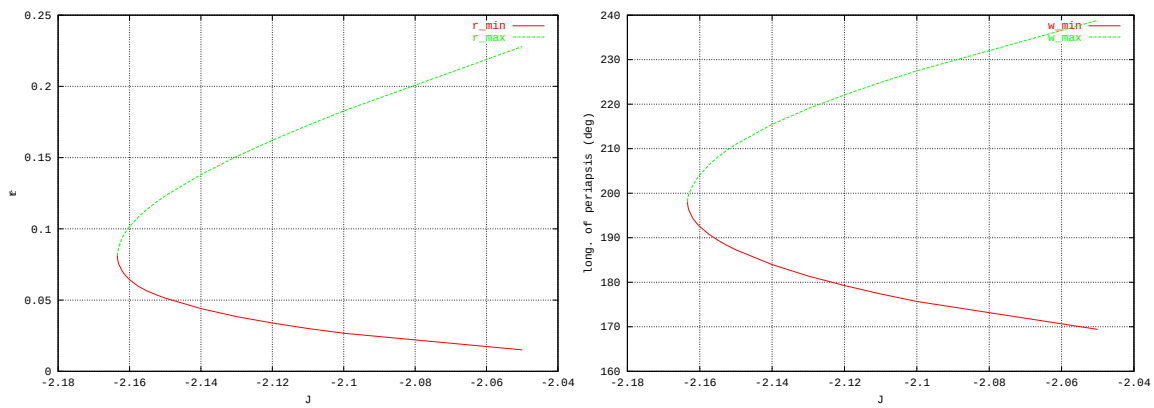

Figure 11: Extrema of radius and longitude of periapsis on Σ_2^a as a function of J (planar case)

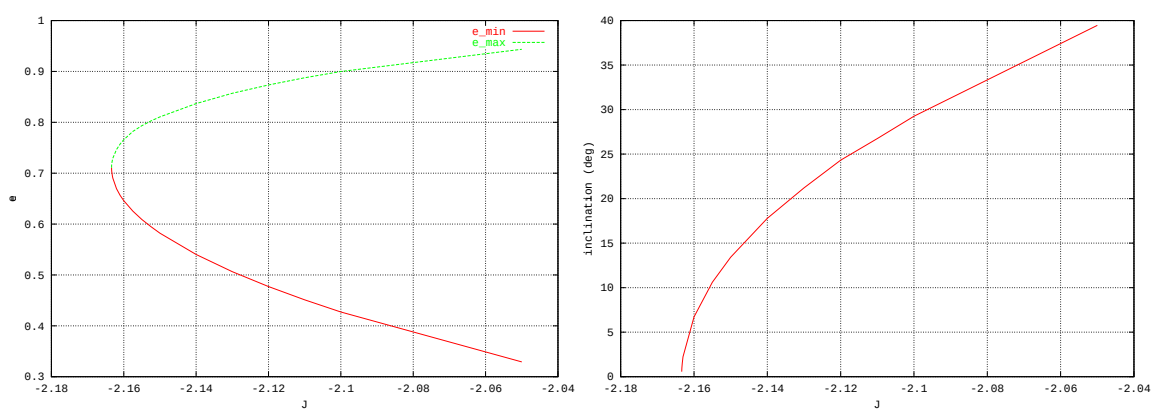

Figure 12: Extrema of eccentricity and inclination on Σ_2^a as a function of J

As noticed earlier, by applying the symmetries S_4 and S_5, the previous results apply for escape through L_1. That is, by taking the symmetry with respect to the origin (in phase space) of the set of points defining the Poincaré maps for L_2, we obtain the Poincaré maps relative to L_1. As concerns the characteristic properties of these maps, only the condition on Ω and $\tilde{\omega}$ are changed by a shift of π.

Similarly, applying S_1 and S_2, we obtain the Poincaré maps relative to the capture problem. Again, nothing changes in the curves given in the Figures 11 and 12, except that Ω tranfroms to $-\Omega$ and $\tilde{\omega}$ transforms to $\pi - \tilde{\omega}$. Here the type of the satellite determines the properties of capture of low energy particles. Type 1 satellites have a large set of trajectories coming from the exterior region

that directly impact the surface of the satellite for values of J close to the critical value J_{L_2}. On the contrary, type 2 satellites capture low energy particles for at least one periapsis without impact. Further backward integration indicates that there is no impact for at least the first three periapsis if J is close enough to J_{L_2}. In the case of Europa, a low energy particle may or may not directly impact the surface.

Figure 13 gives a representation of the different Poincaré maps at $J = -0.35 km^2/s^2$ in the planar case for Europa.

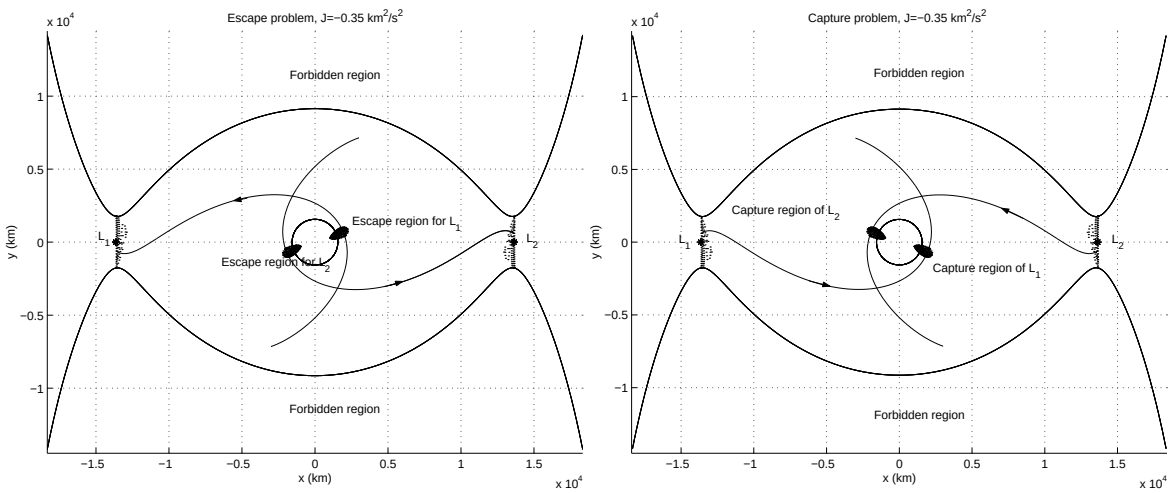

Figure 13: Poincaré maps for escape and capture (case of Europa $J = -0.35 km^2/s^2$)

OPTIMAL TRANSFERS

As mentioned in the introduction, for low altitudes and inclinations, nearly circular orbits present a small periodic variation in eccentricity (see [6]). Therefore, under these conditions we can approximate the motion of a spacecraft by a uniform circular motion and consider what minimum ΔV is needed to escape such a planetary satellite starting in a low circular orbit (or equivalently, be captured into a low circular orbit).

This question can be viewed from two different points of view. The first one asks if there is a particular altitude for which the ΔV to escape is minimal among all direct escape maneuvers starting in low altitude circular orbits. The second assumes the spacecraft is in a low altitude circular orbit and wonders what the minimal ΔV to escape from this given orbit is. With this last problem, one must investigate all the possible techniques to escape starting in a low circular orbit to obtain an optimal escape criterion. The first problem is then answered as a consequence of this criterion and the method used to derive it.

Planar case

Tangential burns are optimal

When in a circular orbit, the ΔV needed to place a spacecraft into an arbitrary trajectory crossing the circular orbit can be expressed as:

$$\Delta V = \mid \vec{v} - \vec{v_{lc}} \mid = \sqrt{v^2 + v_{lc}^2 - 2 v v_{lc} \cos\gamma} \tag{19}$$

where $v_{lc} = \sqrt{\frac{1}{r}}$ is the local circular velocity at a given radius r, $v = \sqrt{2(J + 1/r) + 3x^2}$ is the speed of the arbitrary trajectory and γ is the flight path angle.

From these expressions, it is clear that v and ΔV (parametrized by the Jacobi constant J) increase with J, so that we first look at the minimum value of ΔV for $J = J_{L_2}$. This means that at each point of the stable manifold associated with L_2, we must compare $\vec{v}$ to the local circular velocity and look for the minimum of ΔV.

Figure 14 gives the results of this computation as a function of the radius r. It clearly shows a minimum at periapsis and a rather strong increase around periapsis. This fact can be analytically justifies (see [8]), moreover the result holds for any values of $J \leq 0$ (under some weak restrictions on radius and eccentricity at periapsis). This shows that the minimum ΔV is obtained for tangential burns (i.e. at periapsis) and these maneuvers are hence more optimal than an arbitray non-tangential maneuver. This fact justifies a posteriori the use of the Poincaré maps considered in the previous section to obtain practical optimal criterion for escape.

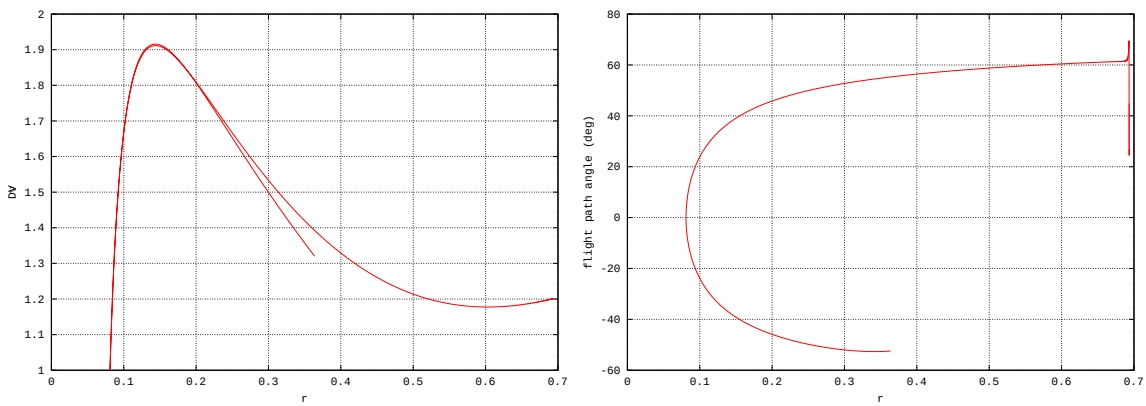

Figure 14: ΔV as computed along the stable manifold associated with L_2

It seems, at this point, that the optimal value of r that minimizes ΔV would be the periapsis of the stable manifold associated with L_2, but the following sections show how to choose better values.

Strategies to escape

In the previous section we showed that along an escaping trajectory the minimum ΔV to escape is reached at periapsis with a tangential burn. Since $\frac{\partial \Delta V}{\partial J} = \frac{1}{v} > 0$ it also shows that this ΔV is the true optimal value if the altitude of the inital circular orbit is exactly equal to the periapsis radius r_{L_2} of the stable manifold of L_2. However, for arbitrary r this case is not met in general. Two strategies for escape are then possible. The first one consists of considering a larger value of J so that the Poincaré map reaches the given radius (i.e., $r \in \Sigma_2^a(J > J_{L_2})$). Then, a tangential burn is applied at the periapsis of an escaping trajectory. We indeed saw in the "Results" section that the range of altitudes reached by the Poincaré map increases as J increases. The second strategy consists of performing a non-tangential burn to place the spacecraft in the stable manifold of L_2. This method is only possible for $r > r_{L_2}$. The figure below illustrates the geometry of the two strategies (Figure 15).

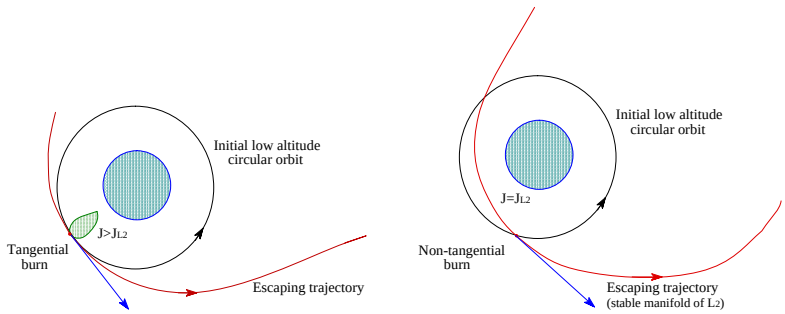

Figure 15: Strategies to escape

Note that in the case $r < r_{L_2}$, only the first strategy is applicable (in the case of single, direct escape transfers).

Let's for now assume $r > r_{L_2}$ and compare these strategies. To do so, we compute the minimum ΔV possible using the first strategy, the ΔV corresponding to the second approach being given in Figure 14.

Minimum ΔV as a function of J

For $J > J_{L_2}$ the Poincaré map is not reduced to a single point and on this set of periapsis, ΔV is a function of radius r and longitude of periapsis $\tilde{\omega}$. We show in [8] that for $r < 0.35$, $\frac{\partial \Delta V}{\partial r} < 0$ and that the minimum ΔV is reached on the boundary of the Poincaré map at a point close to the maximal radius point in the Poincaré map. Denoting $\Delta V_{min}(J)$ this minimal value at a given J, we can numerically compute this value at several values of the Jacobi constant. The altitude r at which ΔV_{min} is reached increases with J so that we can also compute $\Delta V_{min}(r)$ which is more convenient for comparing with Figure 14. Figure16 gives the results of such computations.

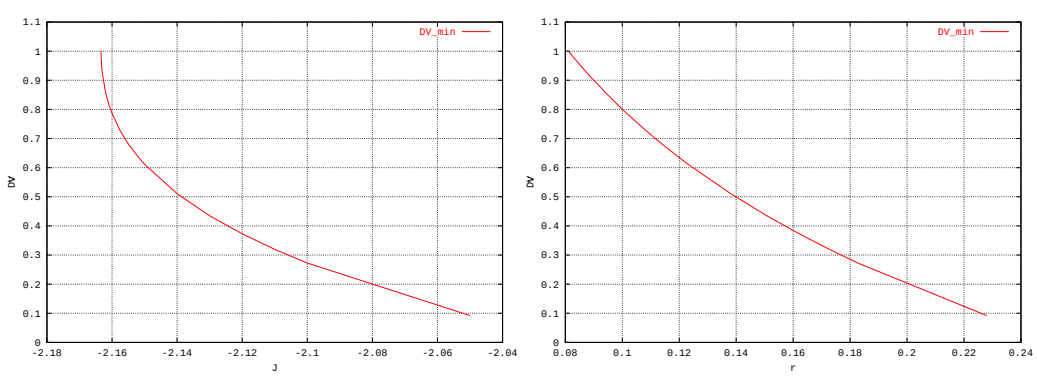

Figure 16: Minimum ΔV for escape as a function of J and r

We clearly see that ΔV_{min} decreases as a function of r. This result allows us to choose the first strategy as being optimal. Indeed, for $J_0 > J_{L_2}$, $\Delta V_{min} \leq \Delta V(r, \tilde{\omega}, J_0)$ where $(r, \tilde{\omega}) \in \Sigma_2^a(J_0)$. Now $\Delta V(r, \tilde{\omega}, J_0) \leq \Delta V_{traj}(r, \tilde{\omega}, J_0)$ where ΔV_{traj} corresponds to the ΔV calculated at any point of an escape trajectory having $(r, \tilde{\omega}, J_0)$ as periapsis (by the optimality of tangential burns). Therefore, $\Delta V_{min}(J_0) \leq \Delta V_{traj}(r, \tilde{\omega}, J_0)$ for any r, $\tilde{\omega}$ in the Poincaré map at a given Jacobi constant J. By the fact that ΔV_{min} decreases as J increases, we see that this inequality is, in fact, satisfied for any $(r, \tilde{\omega}) \in \Sigma_2^a(J \leq J_0)$.

For $J \geq J_0$, we can still show that $\Delta V_{min} \leq \Delta V_{traj}(\bar{r}, \tilde{\omega}, J)$ for any $\bar{r} \leq r$ and any $\tilde{\omega}$ (see [8]).

This proves the global optimality of ΔV_{min} among all one-impulse maneuvers. We can moreover prove that ΔV_{min} is, in fact, optimal among a larger class of two impulses maneuvers (see [8]).

Optimal criterion

Gathering all the results proven in the previous sections, we obtain the following escape criterion:

Starting in a low circular orbit, at a given radius $r > r_{L_2}$, the minimum ΔV needed to directly escape is given $\Delta V_{min}(r)$ (see Figure 17). The impulsive thrust must be tangential to the path and the placement of the maneuver is determined by $\tilde{\omega}(r)$, given in Figure 17.

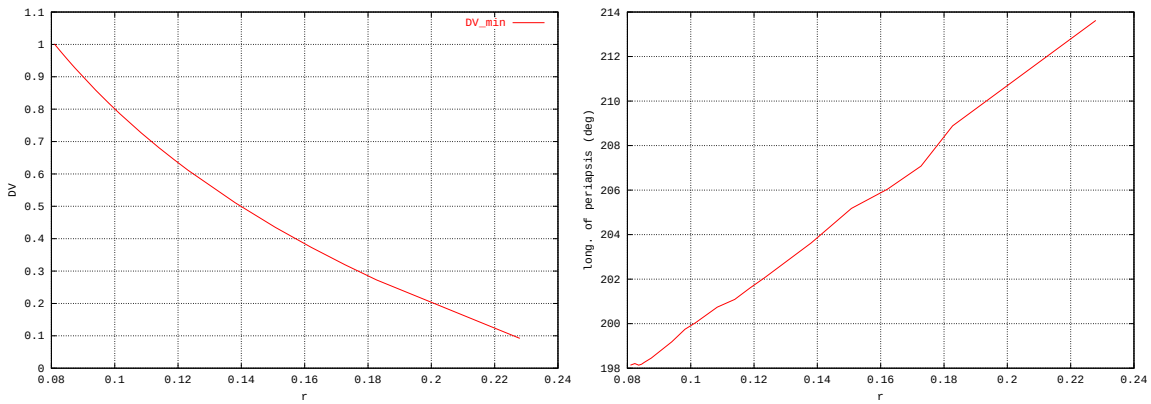

Figure 17: Optimal ΔV and longitude of periapsis for escape for $r > r_{L_2}$

Applying a tangential burn at a given point fixes the elements of the transfer trajectory at periapsis. Therefore, at the time of the maneuver, $\tilde{\omega}$ is equal to the polar angle (which is approximated by Nt in a circular orbit).

For $r < r_{L_2}$, the minimum ΔV to escape is reached near the point r_{min} (see [8]). The values of ΔV and $\tilde{\omega}$ as a function of r are given in Figure 18.

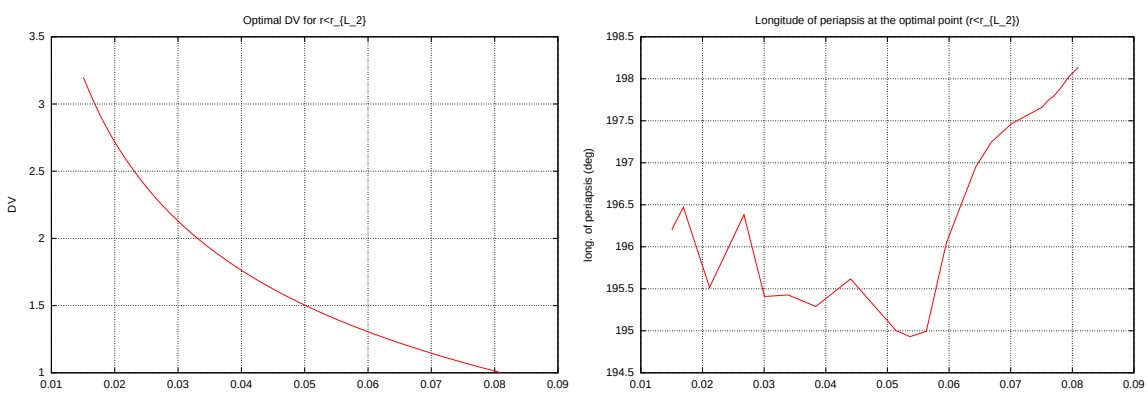

Figure 18: Optimal ΔV and longitude of periapsis for escape for $r < r_{L_2}$

Note that this optimal escape criterion is sufficient and necessary. In particular, escape is always achieved for a tangential $\Delta V > \Delta V_{opt}$. This condition indeed implies that $J > J_{opt}$ and $\Sigma_2^a(J) \supset \Sigma_2^a(J_{opt})$. The optimal point at Jacobi constant J_{opt} hence lies inside $\Sigma_2^a(J)$, and is still the periapsis

of an escape trajectory.

This last result may prove useful for applications since it is the expression of a stability of the escape relative to errors in the initial thrust. In fact, since the optimal point is not isolated, small errors in thrust directions correspond to placing the spacecraft on an escaping trajectory with periapsis near the optimal value. That is, escape maneuvers are also robust to small errors in thrust directions.

Figure 17 shows, moreover, that the answer to the first initial question is negative: there is no optimal value of r such that ΔV is minimal among all directly escaping transfers for low circular orbits. In fact, one can show that there is a minimum for $r > 0.44$ (corresponding to $\frac{\partial \Delta V}{\partial r} = 0$), but the assumption for a spacecraft to be in a circular orbit is not valid anymore and the definition of ΔV is less meaningful.

Applying the previous results to Miranda, Europa, Titan and Triton, we can compute the minimal ΔV to escape from these planetary satellites starting in a circular orbit at a low altitude ($h \simeq 0$). The savings compared to a Keplerian escape maneuver (parabolic trajectory) are also computed and summarized in Table 2:

Table 2: Minimum ΔV to escape the surface of Miranda, Europa, Titan and Triton

Satellite	ΔV scale factor (m/s)	Nondimensional ΔV	ΔV to escape (m/s)	Savings when comp. to Kepler. (m/s)
Europa	403.4	1.03	415.5	176.3[1]
Titan	344.7	1.96	675.6	97.9
Miranda	62.5	0.2	12.5	45.4
Triton	475.4	1.63	774.9	147.3

Non-planar case

As noticed in section "Results", the extrema of r, Ω and i over Σ_2^a are reached at some point in the equatorial plane ($z = 0$) (see Figure 19). This is still true for ΔV, for which the minimal value is reached at $r \simeq r_{max}$. The previous optimal criterion is therefore still valid in 3 dimensional space. However in this case, one can ask what is the minimum ΔV to escape starting in a non-zero inclination initial orbit.

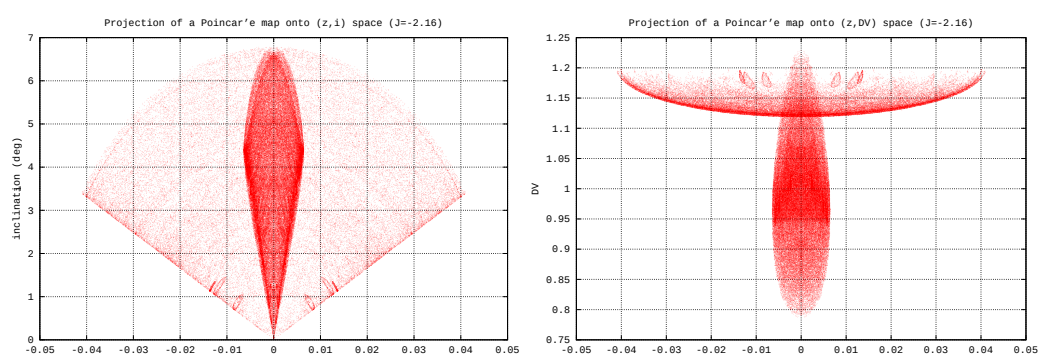

Figure 19: Extrema of inclination and ΔV are reached in the equatorial plane

[1]Savings of $190m/s$ are obtained when starting in a $200km$ altitude circular orbit

Variations in inclination

As J varies, the ranges of inclination reached by the Poincaré maps increase, reaching rather large values for large values of J (see Figure 12).

The radius where the maximal inclination is reached decreases with J. However, it is still true that at any fixed r, the maximum in inclination increases with J. Figure 20 gives a series of Poincaré maps at several values of Jacobi constant, projected onto the (r, i) space.

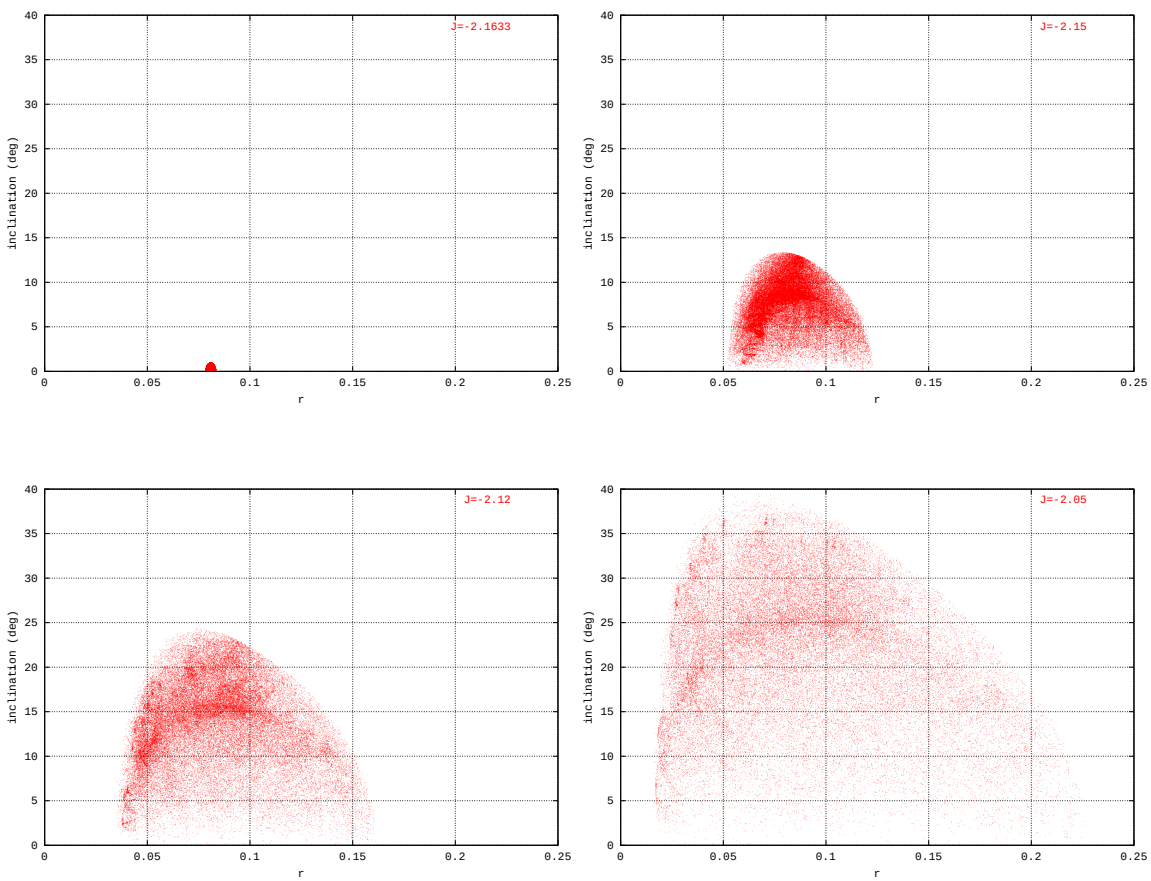

Figure 20: Projection of a few Poincaré maps (Σ_2^a) onto the (r, i) space

Strategy to escape starting in a non-zero inclined orbit

We have seen in the planar case that tangential maneuvers are more optimal than non-tangential ones. This results still holds in the 3 dimensional case (see[8]), leading us to choose the same approach to the problem as in the planar case (see section "Planar case _ Strategies to escape").

Starting from a non-zero inclination, low altitude, circular orbit (determined by the radius r and the inclination i), the strategy to escape consists of increasing J so as the maximal inclination reached by the Poincaré map at the given radius r equals the initial inclination i. Then, a tangential maneuver is applied at this point of maximal inclination (at fixed radius r). Since we know that this maximum is reached in the equatorial plane ($z = 0$), we have the condition $\omega = 0^o$ at the time of the maneuver. Presently, no condition has been obtained for Ω. This will be corrected in the near future.

Next arises the question of the optimality of such an approach, for which no definite result is given in this paper. However, Figure 21 presents the projection of a few Poincaré maps onto the $(r, \Delta V)$

space and we can see that at any fixed radius r and Jacobi constant J, the variations of ΔV over the cross-section of the corresponding Poincaré map are very small (less than 0.05 in the worst case at $J = -2.05$). As J increases, ΔV increases at any fixed point. These results allow us to conclude that, in the case of non-optimality of the previous approach, the value obtained is very close to the true optimum.

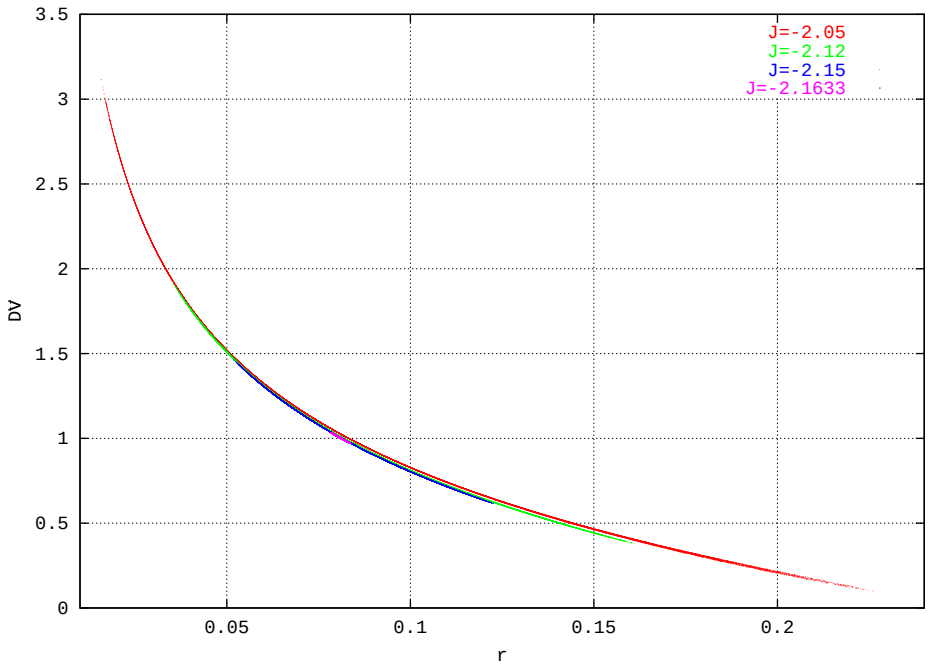

Figure 21: Projection of a few Poincaré maps onto the $(r, \Delta V)$ space

Operation of the maneuver

The previous discussion proved the existence of an optimal ΔV to escape starting at an inclination i. This ΔV is well approximated by the values given in Figure 21 and this may be sufficient from a pratical point of view (less than $20m/s$ error in the case of Europa if the approach described above is not optimal). We also saw that this optimum is reached for $\omega = 0^o$. No condition has been given for Ω except for the bounds given in Figure 11.

From a theoretical point of view we know, however, that whatever the optimal value for Ω is, it can be targetted with an arbitrary precision by correctly choosing the time of the maneuver. Indeed, the position of the spacecraft at the time of the maneuver fixes ω and Ω at the periapsis of the escape trajectory. Therefore, as any given time, we can associate the position of the spacecraft in its inital orbit with some values of ω and Ω that would correspond to the values taken if the maneuver was actually performed at that time. We hence obtain two functions of time $\omega(t)$ and $\Omega(t)$. Since the initial orbit is assumed circular and the frame is rotating, the point $(\omega(t), \Omega(t))$ draws a line on the torus space $[0, 2\pi]^2$, which indicates that any value of ω and Ω can be reached to arbitrary precision by waiting for a sufficiently long time (assuming that the slope of the line $(\omega(t), \Omega(t))$ is irrational).

CONCLUSION

The structure of escaping and capture trajectories in the Hill three body problem has been investigated using a Poincaré map. The extrema characterizing the set of periapsis obtained (r, Ω and i) has been shown to be reached in the equatorial plane and their variation as a function of the Jacobi constant has been given. These results have been applied to the problem of determining the minimum ΔV needed to escape from a planetary satellite, starting in a low altitude circular orbit. An optimal criterion hass been given in the planar case and a practical approach has been given in the three dimensional case. It is shown that the resulting cost for escape decreases as the initial altitude increases. The cost to escape in the vicinity of a planetary satellite is on the order of the ΔV scale factor, $(\mu N)^{1/3}$, (which equals the cost to escape at the periapsis of the stable manifold associated with L_1 or L_2). Future work will try to characterize more fully the optimality in the three dimensional case. A better inderstanding of the apparent separation of the Poincaré map into two disjoint sets and the study of Poincaré maps between previous periapsis passages are also further topics to be explored.

ACKNOWLEDGEMENT

The work described was funded by the TMOD Technology Program and Outer Planets/Solar Probe Project by grants from the Jet Propulsion Laboratory, California Institute of Technology which is under contract with the National Aeronautics and Space Administration.

References

[1] V.I. Arnol'd, editor. *Dynamical systems III.* Encyclopedia of Mathematical Sciences. Springer-Verlag, 1988.

[2] J.A. Burns and M.S.Matthews, editors. *Satellites.* The University of Arozona Press, Tuscon, 1986.

[3] M. Hénon and J.M. Petit. Series Expansions for Encounter-type Solutions of Hill's Problem. *Celest. Mech. & Dyn. Astr.*, 38:67–100, 1986.

[4] M.Hénon. Numerical Exploration of the Restricted Problem.V. Hill's case: Periodic Orbits and their Stability. *Astron. & Astrophys.*, 1:223–238, 1969.

[5] Oliver Montenbruck and Eberhard Gill. *Satellite Orbits: models, methods, and applications.* Springer, 2000.

[6] D.J. Scheeres, M.D. Guman, and B.F. Villac. Stability analysis of planetary satellite orbiters: Application to the Europa Orbiter. *Journal of Guidance, Control and Dynamics*, 24(4), July-August 2001.

[7] S.Wiggins. *Introduction to Applied Nonlinear Dynamical Systems and chaos.* Springer-Verlag, 1990.

[8] B.F. Villac and D.J. Scheeres. Structure of escape and capture trajectories in the Hill three body problem and Applications. In preparation.